NIH Public Access
Author Manuscript
ACS Chem Biol. Author manuscript; available in PMC 2013 November 16.

Published in final edited form as:
ACS Chem Biol. 2012 November 16; 7(11): 1830–1839. doi:10.1021/cb3003013.

Paroxetine Is a Direct Inhibitor of G Protein-Coupled Receptor Kinase 2 and Increases Myocardial Contractility

David M. Thal[1], **Kristoff T. Homan**[1,†], **Jun Chen**[2,†], **Emily K. Wu**[1], **Patricia M. Hinkle**[3], **Z. Maggie Huang**[4], **J. Kurt Chuprun**[4], **Jianliang Song**[4], **Erhe Gao**[4], **Joseph Y. Cheung**[4], **Larry A. Sklar**[2], **Walter J. Koch**[4], and **John J.G. Tesmer**[1,*]

[1]Life Sciences Institute and the Department of Pharmacology, University of Michigan, Ann Arbor, Michigan 48109

[2]Center for Molecular Discovery, University of New Mexico Health Sciences Center, Albuquerque, New Mexico 87131

[3]Department of Pharmacology and Physiology, University of Rochester Medical Center, Rochester, New York 14642

[4]Center for Translational Medicine, Temple University School of Medicine, Philadelphia, Pennsylvania 19140

Abstract

G protein-coupled receptor kinase 2 (GRK2) is a well-established therapeutic target for the treatment of heart failure. Herein we identify the selective serotonin reuptake inhibitor (SSRI) paroxetine as a selective inhibitor of GRK2 activity both *in vitro* and in living cells. In the crystal structure of the GRK2·paroxetine-Gβγ complex, paroxetine binds in the active site of GRK2 and stabilizes the kinase domain in a novel conformation in which a unique regulatory loop forms part of the ligand binding site. Isolated cardiomyocytes show increased isoproterenol-induced shortening and contraction amplitude in the presence of paroxetine, and pretreatment of mice with paroxetine before isoproterenol significantly increases left ventricular inotropic reserve *in vivo* with no significant effect on heart rate. Neither is observed in the presence of the SSRI fluoxetine. Our structural and functional results validate a widely available drug as a selective chemical probe for GRK2 and represent a starting point for the rational design of more potent and specific GRK2 inhibitors.

*Corresponding author: tesmerjj@umich.edu.
†Equal contribution

Accession Codes. The atomic model and structure factors for GRK2·paroxetine-G$\beta_1\gamma_2$C68S have been deposited with the Protein Data Bank as entry 3V5W.

Author Contributions. D.M.T. contributed to the experimental design, protein production, HTS implementation, crystallization and structure determination of the GRK2·paroxetine complex, flow cytometry assays, Thermofluor assays, rhodopsin phosphorylation assays, and writing the manuscript. J.C. and L.S. to assay adaptation, HTS implementation, dose-response confirmation, analysis of data from the Prestwick Chemical Library and writing the manuscript. K.T.H. and E.W. to flow cytometry assays, rhodopsin and tubulin phosphorylation, and Thermofluor assays. P.M.H. contributed the cell-based TRH phosphorylation assay. W.J.K, J.C.C., J.S., Z.M.H., E.G. and J.K.C. contributed to the experimental design of the ventricular myocyte and *in vivo* inotropy measurements, and W.J.K. to the writing the manuscript. J.J.G.T. to the experimental design, crystal structure refinement, and writing the manuscript.

Competing Financial Interests Statement. L.A.S. is a founder of IntelliCyt, which produces the HyperCyt high-throughput flow cytometry platform.

Supporting Information Available: Supplementary methods, supplementary figures 1–6, and supplementary tables 1–2 are available free of charge via the Internet at http://pubs.acs.org.

$watermark-text
$watermark-text
$watermark-text

$watermark-text

$watermark-text

$watermark-text

The speed and strength of myocardial contraction is regulated by the sympathetic nervous system via the catecholamine hormones epinephrine and norepinephrine, which act on β-adrenergic receptors (βARs) to increase intracellular adenosine 3′,5′-monophosphate (cAMP) (1). Prolonged sympathetic stimulation of βARs results in receptor desensitization and uncoupling from heterotrimeric G proteins, a process initiated by phosphorylation of activated receptors by G protein-coupled receptor kinases (GRKs) (2). Under normal physiological conditions this system plays a critical role in maintaining homeostasis of blood supply, as persistent βAR signaling is detrimental (3–5).

One of the defining characteristics of heart failure is impairment of the myocardial βAR system (6). In the failing heart, the loss of cardiac output promotes increased levels of circulating catecholamines, resulting in severe uncoupling of βARs and a loss of inotropic reserve (7). This desensitization and uncoupling coincides with a 2–3 fold increase in GRK2 activity accompanied by an increase in both protein and mRNA levels (8, 9). Studies in mice overexpressing GRK2 in the heart show attenuation of isoproterenol-stimulated contractility, reduced cAMP levels, and impaired cardiac function (10). As such, it has been hypothesized that inhibition of GRK2 function would be beneficial during heart failure (11). Indeed, studies in animal models with the GRK2 inhibitory protein, βARKct, or with cardiac-specific GRK2 gene deletion, have shown that inhibition of GRK2 or lowering expression improves heart failure outcome (12–16).

Consequently, there has been considerable interest in developing GRK2 selective small molecule inhibitors. The natural product balanol inhibits GRK2 in the low nanomolar range, but is a non-selective inhibitor of the protein kinase A, G and C family (AGC kinases) (17, 18). Other inhibitors of GRKs have also been described, but these either have poor potency (19), low selectivity (20), or have non-drug like properties (21). Takeda Pharmaceuticals, Inc. have developed potent inhibitors selective for the GRK2/3 subfamily (22) that bind in the active site of the enzyme (23), but these have not advanced to clinical trials.

Recently, an RNA aptamer (C13) was developed that selectivity inhibits GRK2 activity with nanomolar potency (24). Although RNA aptamers are generally not considered to be viable therapeutics for oral therapy, they can be used to identify small molecules with similar properties in aptamer-displacement assays (25). Herein, we describe the development of such an assay by which we discovered that the Food and Drug Administration (FDA) approved drug paroxetine (Paxil®) as a relatively potent inhibitor of GRK2 activity both *in vitro* and in living cells that exhibits up to 60-fold selectivity over other GRKs. Crystallographic analysis demonstrated that paroxetine stabilizes a unique and atypically well-ordered conformation of GRK2. Furthermore, we showed that paroxetine, but not the chemically unrelated SSRI fluoxetine (Prozac®), increased contractility in isolated cardiomyocytes and myocardial βAR inotropic reserve in living mice, consistent with GRK2 inhibition.

RESULTS AND DISCUSSION

Discovery of GRK2 inhibitors by aptamer displacement

The crystal structure of GRK2 in complex with a variant of C13 (C13.28) showed that the aptamer stabilizes the GRK2 kinase domain in a unique conformation by forming extensive interfaces both within and outside the active site (26). Thus, compounds that displace C13.28 from GRK2 may also stabilize a unique state or bind in a non-canonical manner. To measure aptamer binding to GRK2, we used a bead-based flow cytometry interaction assay that has been previously used to study protein-protein interactions with GRK2 (27) as a high-throughput screen (HTS) (28). GRK2 was first biotinylated (bGRK2) and then immobilized on streptavidin coated microspheres that are then incubated with fluorescein

$watermark-text

$watermark-text

$watermark-text

labeled C13.28 (C13.28-FAM) (Figure 1a). Compounds that inhibit aptamer binding can then be identified by their ability to decrease the fluorescence of the microspheres as they pass through a flow cytometer.

We first tested the assay against a panel of known GRK ligands including unlabeled aptamer, ATP, the adenosine analog sangivamycin (29), and the Takeda compound 103A (Figure 1c). The aptamer and 103A were fully efficacious and potent inhibitors of C13.28-FAM binding (Table 1). ATP and sangivamycin, however, were only able to compete off 40–70% of the aptamer indicating that these lower affinity compounds (K_m of 28 μM for ATP (23) and a half-maximum inhibitory concentration (IC_{50}) of 70 μM for sangivamycin (29)) are only partially capable of displacing the aptamer, resulting in an apparent loss of affinity between GRK2 and C13.28-FAM.

We next screened ~40,000 compounds using the aptamer displacement assay at the University of Michigan Center for Chemical Genomics. Although this screen identified no strong leads, the assay exhibited excellent statistics (Z′ of 0.8–0.9 based on the positive and negative controls). We additionally tested our assay against the 1200 compound Prestwick Chemical Library (Supplementary Table 1), which primarily contains FDA approved drugs, at the University of New Mexico Center for Molecular Discovery. Two hits, paroxetine hydrochloride (P-851) and 4-hydroxy-quinone monohydrate (P-835) were identified (Figure 1d,e).

Paroxetine binds directly to GRK2 and inhibits kinase activity

The potencies of P-835 and P-851 were determined by competition against 2 nM C13.28-FAM using the flow cytometry assay. P-835 competed with aptamer binding with a −log IC_{50} (pIC_{50}) of 5.5 ± 0.4 and a Hill slope of −1.6. P-851 only partially inhibited aptamer binding (~70%) with a pIC_{50} of 4.5 ± 0.2 and a Hill slope of −0.7 (Figure 1f, Table 1). As a counter screen, the compounds were tested for their ability to diminish the fluorescence of bead-bound biotinylated C13.28-FAM (bC13.28-FAM). However, neither compound significantly diminished bead-bound fluorescence in this assay (Supplementary Figure 1).

In the displacement assay, compounds could inhibit by binding either to GRK2 or the aptamer. To test for direct binding to GRK2, we utilized a thermal stability assay that measures the ability of a ligand to increase the melting temperature (T_m) of a protein (Figure 1g, Table 1). In buffer alone, GRK2 exhibited a T_m of 37 °C. Addition of 200 μM Mg^{2+}·ATP induced a 5 °C increase. In comparison, 10 μM balanol or Takeda compound 103A increased the T_m by 12–19 °C (23). Addition of 200 μM P-835 increased the thermal stability by only 1 °C suggesting that if it binds, it does so only weakly. However, at the same concentration P-851 increased the thermal stability of GRK2 by 8 °C, indicating that it not only binds directly to GRK2, but also stabilizes the enzyme to a greater extent than ATP.

We next tested the ability of P-835 and P-851 to inhibit GRK2 mediated phosphorylation of light activated rhodopsin, a canonical and readily available GPCR, in rod outer segment (ROS) membranes. In the presence of 5 μM ATP, only P-851 was able to inhibit GRK2, doing so with a pIC_{50} of 4.7 ± 0.04 (n=4; Figure 2a). DMSO alone had no effect (Supplementary Figure 2a). Given that P-835 had no effect on inhibiting GRK2 kinase activity and only a small effect on GRK2 thermostability, it was not further studied. Because GRKs can also be inhibited by blocking their recruitment to membranes (30), we used the soluble substrate tubulin to directly probe inhibition of catalytic activity (31, 32). Paroxetine inhibited GRK2 phosphorylation of tubulin with a pIC_{50} of 5.6 ± 0.07 (Figure 2b, Table 2).

$watermark-text

$watermark-text

$watermark-text

Paroxetine is a selective inhibitor of GRK2

To characterize the selectivity of P-851 (henceforth referred to as paroxetine) we tested its ability to thermostabilize GRK1 and GRK5, representative members of the two other vertebrate GRK subfamilies (33). Addition of 200 μM ATP increased the T_m by 18 and 7 °C, respectively, for GRK1 and GRK5. However, neither 200 μM paroxetine nor P-835 significantly changed the thermal stability of GRK1 and GRK5 (Figure 1g, Table 1). Thus, paroxetine selectively thermostabilizes GRK2. We then tested the ability of paroxetine to inhibit phosphorylation of ROS by GRK1 and GRK5, determining pIC_{50} values of 3.5 ± 0.01 (n=3) and 3.6 ± 0.3 (n=3), respectively (Figure 2a, Table 2). Thus, paroxetine exhibits 16- and 13-fold lower potency towards GRK1 and GRK5, respectively, in this assay. When tubulin was used as the substrate, paroxetine inhibited GRK1 and GRK5 activity with pIC_{50} values of 3.8 ± 0.05 and 3.9 ± 0.06, corresponding to 60 and 50-fold lower potencies compared to GRK2, respectively.

Paroxetine inhibits phosphorylation of the TRH receptor by GRK2

We next examined if paroxetine could inhibit GRK2 activity in HEK293 cells. The thyrotropin-releasing hormone (TRH) receptor undergoes rapid ($t_{1/2}$=15 s) and quantitative agonist and GRK2-dependent phosphorylation on its cytoplasmic C-terminus (34). Paroxetine inhibited the initial rate of TRH-dependent phosphorylation almost completely with an IC_{50} of ~31 μM (Figure 2c). Thus, paroxetine can cross biological membranes and inhibit GRK2-specific phosphorylation of a GPCR at a functionally relevant site in living cells.

Paroxetine reorganizes the active site of GRK2

To understand the molecular basis for paroxetine inhibition of GRK2, we co-crystallized paroxetine with the GRK2-Gβγ complex and solved its atomic structure using diffraction data extending to 2.07 Å spacings (Supplementary Table 2, Supplementary Figure 3a). Paroxetine binds in the active site of GRK2 in a manner that overlaps the adenosine and ribose sub-binding sites of ATP (Figure 3a,b) (35). In the adenosine subsite, one of the dioxole oxygens mimics the N1 atom of the substrate ATP by forming a hydrogen bond with the amide backbone nitrogen of Met274 (Figure 3b,c). In the ribose subsite, the secondary amine on the piperidine moiety of paroxetine contributes to a network of hydrogen bonds formed by the carboxylic acid of Asp278, the carbonyl oxygen of Ala321, the carboxamide of Asn322 and a water molecule (Figure 3b,d). The binding of paroxetine to GRK2 is further stabilized by an additional 18 nonpolar interactions, with the fluorophenyl substituent of paroxetine packing into a cavity formed between residues in the P-loop and the side chains of Lys220 and Leu222 (Figure 3b, Supplementary Figure 4.

In the GRK2-paroxetine structure, the relative orientation of the small and large lobes of the kinase domain changes by 3.5° relative to apo-GRK2, resulting in a conformation distinct from that observed in prior GRK2 structures (Supplementary Figure 3b). In addition, residues 475–484 within the so-called active site tether (AST) of GRK2 become ordered in the paroxetine complex. The AST is a region within the C-terminal tail found in AGC kinases that passes between the large and small lobes and typically only becomes ordered when the kinase domain exhibits a more active conformation. Because it contributes directly to the active site, it is thought to be a potential locus for regulatory control (36). Residues 471–477 of the GRK2 AST adopt a similar conformation to the analogous residues of GRK6 (466–472) when in complex with sangivamycin (37). However, the remaining visible residues of the GRK2 AST (residues 478–484), which diverge in sequence and structure from those of GRK6, pack between the small and large lobes. Residues 480–482 extend the β-sheet of the small lobe via backbone hydrogen bonds with Arg199 and pack on top of the central piperidine ring of paroxetine (Figure 3e). Preceding these residues, Ala479 seems to

$watermark-text

$watermark-text

$watermark-text

make a key anchoring interaction by packing against Tyr281 in the αD helix and forming a hydrogen bond with the backbone amide of Asp278, just C-terminal to the hinge of the kinase domain (Figure 3d).

Analogs of paroxetine bind with predictably lower affinity to GRK2

Based on the GRK2·paroxetine-Gβγ structure, loss of fluorine in defluoro paroxetine was predicted to reduce the affinity of paroxetine for GRK2 through the loss of multiple hydrophobic interactions (Figure 3a,b), whereas the loss of a methylene in desmethylene paroxetine was predicted to potentially reduce favorable van der Waals interactions in the adenine subsite (Figure 3b,c; Supplementary Figure 5a). Both paroxetine derivatives exhibited a significant loss in their ability to thermostabilize GRK2 and exhibited diminished binding affinity (Supplementary Figure 5b,c). Defluoro and desmethylene paroxetine had 5–8 fold and 2.5–3.5 fold decreases in pIC_{50}, respectively, depending on the substrate (Supplementary Table 3).

Paroxetine increases myocardial contractility

We next examined whether paroxetine could affect the activity of GRK2 in a physiologically relevant system by testing if paroxetine could influence isolated adult mouse ventricular myocyte contractility at baseline and in response to βAR stimulation. Compared to untreated cells, isoproterenol significantly enhanced sarcomere shortening and contraction amplitude, demonstrating a normal response to βAR agonism (Figure 4a,b). Interestingly, pretreatment of the cells with 10 μM paroxetine for 10 min did not alter baseline myocyte functional parameters or shape, and significantly potentiated the isoproterenol effects on contractility compared to isoproterenol alone (Figure 4c, Table 3). These data are consistent with effects of other GRK2 inhibitors in myocytes, either via βARKct expression (38) or pretreatment with M119, a compound recently shown to disrupt Gβγ-mediated GRK2 membrane translocation and activity (39).

We then tested the effects of paroxetine on *in vivo* cardiac inotropy in wild-type mice (Figure 5a). Using catheter-mediated hemodynamic measurements we found that IV injection of 10 mg kg^{-1} paroxetine to mice produced a small immediate increase in left ventricular (LV) dP/dt, a measurement of cardiac contractility, but more importantly, a significant increased response to isoproterenol was evident, shifting the βAR-mediated inotropy dose-response curve (Figure 5b,c). Importantly, no significant change in heart rate was seen (Figure 5d), which has also been observed *in vivo* with βARKct expression (10, 16). Therefore, application of paroxetine to myocytes in culture and *in vivo* can increase βAR-mediated contractility, consistent with direct GRK2 inhibition.

Fluoxetine does not inhibit GRK2 activity or myocyte contractility

We next tested if the chemically unrelated SSRI fluoxetine could elicit the same effects as paroxetine. Fluoxetine did not inhibit ROS phosphorylation by GRK2 (Supplementary Figure 2b), and had negligible effects in the cardiomyocyte contractility assay (Supplementary Table 4). Furthermore, fluoxetine also had no effect on *in vivo* βAR-mediated cardiac contractility when mice were pre-treated with the drug (Supplementary Figure 6). Thus, the enhancement of cardiac contractility by paroxetine is not likely due to its ability to inhibit serotonin reuptake.

Discussion

Over the past 20 years, major attention has been focused on developing highly selective kinase inhibitors, an area that now accounts for over 25% of all pharmaceutical drug targets (40). Conventional drug discovery programs have aimed at developing kinase inhibitors

based on enzymatic reactions, which are prone to discovering nonselective ATP competitive inhibitors because the assay is designed to target the highly conserved protein kinase active site (41). The discovery of a RNA aptamer, which selectively inhibits GRK2 with nanomolar affinity by stabilizing a unique inactive conformation (24, 26), has allowed us to perform an orthogonal screen in which we could potentially identify similarly selective compounds that bind to GRK2 in a non-canonical way or stabilize unique states incompatible with aptamer binding.

Our preliminary screens identified paroxetine, one of the most potent SSRIs, as an inhibitor of GRK2, with up to 60-fold selectivity over other GRK subfamilies. Direct binding to GRK2 was verified via shifts in its thermostability and by inhibition of ROS and tubulin phosphorylation *in vitro*. Effectiveness in living cells was demonstrated by the ability of paroxetine to inhibit GRK2-specific phosphorylation of the TRH receptor, and to enhance contractility in isolated murine cardiomyocytes as well as in a live animal. Another SSRI with a different chemical scaffold, fluoxetine, had no effect in our *in vitro* kinase assays or on myocyte contractility *ex vivo* or *in vivo*. These data all indicate that paroxetine is not only a highly potent SSRI, but also an effective inhibitor of GPCR phosphorylation and desensitization via direct binding to GRK2.

We also determined the crystallographic structure of the GRK2·paroxetine-Gβγ complex. Paroxetine interacts with the active site of the kinase in a manner that overlaps with the ATP binding site and stabilizes a conformation of GRK2 that has not been previously observed. Despite the fact that the AST of GRK2 is partially ordered in this structure, it is unlikely to represent a more active configuration of GRK2 because the small and large lobes, and hence its catalytic machinery, are still misaligned from what is expected to be their active configuration (37). This novel conformation of GRK2, in which non-conserved residues from the AST contribute to the ligand binding site, is likely responsible for the large observed ΔT_m upon ligand binding compared to other GRKs as well as to its selectivity. Thus, the structure represents a unique scaffold for the rational design of selective drugs for GRK2, based on either the paroxetine scaffold or on other classes of inhibitors that can stabilize the same state. Notably, paroxetine is a relatively small drug (329.3 Da) that could readily be modified and still retain drug-like properties.

Interestingly, paroxetine was an 8-fold more potent inhibitor of tubulin phosphorylation than of ROS. Previous studies suggest that activated rhodopsin and other receptors allosterically activate GRK2 (42) by inducing a conformational change in the kinase domain that aligns the catalytic machinery (37). Thus, an explanation for the observed difference in potency is that when GRK2 is recruited to the membrane and interacts with receptors, its conformation is less compatible with paroxetine binding. In comparison, tubulin is a relatively inefficient substrate and is not expected to exert the same allosteric effect on GRK2 (32). This hypothesis is consistent with the observation that the structure of the GRK2·paroxetine complex does not seem to be catalytically competent.

Paroxetine has been on the market since 1992. Steady state blood plasma levels of the drug in healthy male adults is estimated to be 125 nM (43), which is 1–2 log units below the pIC_{50} we measure for inhibition of GRK2 activity. However, only 1% remains in the plasma and the drug widely distributes throughout the body, including the CNS, where local concentrations of the drug could be higher. The use of paroxetine use has not been correlated with large cardiovascular changes, although there have been reports of increased cardiovascular defects in newborns whose mothers were taking paroxetine (44) leading to a black box warning and pregnancy category D labeling. Indeed, deficiency in GRK2 is well known for embryonic lethal cardiovascular defects in mice (45), but the causal relationship between these two observations is not known. Studies on improvement in heart function in

$watermark-text $watermark-text $watermark-text

$watermark-text

$watermark-text

$watermark-text

patients treated with paroxetine are not obvious from the literature, except that paroxetine use in depressed patients has not led to significant cardiotoxic events (46, 47). However, our current results would seem to warrant a clinical study to assess heart failure outcomes in patients that receive paroxetine for depression, especially in comparison with heart failure patients treated with other SSRIs.

In summary, we have used a novel HTS strategy for identifying a kinase inhibitor in which compounds were selected for their ability to displace a selective RNA aptamer from GRK2. This approach has identified paroxetine as a selective inhibitor of GRK2 that functions both *in vitro* and *in vivo*. Our data indicates that future, more potent variants of paroxetine, or novel chemicals modeled into the novel conformation of the GRK2·paroxetine complex, have great potential as unique chemical probes and, ultimately, as new therapeutic leads for the treatment of heart failure.

METHODS

Purification of recombinant proteins

Human GRK2-S670A and C-terminal hexahistidine tagged bovine $GRK1_{535}$ and $GRK5_{561}$ were expressed and purified as previously described (23). Soluble bovine $G\beta_1\gamma_2$C68S, which lacks the geranylgeranylation site at the C-terminus of $G\gamma_2$, was also expressed and purified as previously described (48).

Flow cytometry based bead binding assay

The assay was performed on an Accuri C6 flow cytometer equipped with a HyperCyt Autosampler as previously described (27), but with modifications as described in Supplementary Methods.

HTS

High-throughput screening against the GRK2–aptamer interaction was carried out at the Center for Chemical Genomics (University of Michigan) and at the University of New Mexico Center for Molecular Discovery, as previously described (28).

Phosphorylation assays

GRK mediated phosphorylation of light-activated bovine rod outer segments (ROS), or cuttlefish Sepia rhodopsin in cholate insoluble membranes, was performed essentially as previously described with 10 nM GRK, 100 μM ATP and 5 μM ROS, or 5 μM ATP and 500nM ROS in the bovine rhodopsin reactions and with 50 nM GRK2, 100 μM ATP and 20 μM rhodopsin in the *Sepia* reactions (23). Phosphorylation of tubulin was performed analogously with 50 nM GRK, 5 μM ATP and 500 nM tubulin. GRKs were incubated with increasing concentrations of paroxetine or paroxetine analogs (from 100 mM stock solutions in 100% DMSO) for at least 30 min prior to starting the reaction with ATP. Data was analyzed as described in the Supplementary Methods.

Crystallization and structure determination

Human GRK2 (1.9 mg) and bovine $G\beta_1\gamma_2$C68S (1.5 mg) were gel filtered into 20 mM HEPES pH 8.0, 50 mM NaCl, 5 mM $MgCl_2$, and 2 mM DTT, and then mixed together and concentrated to 8 mg ml^{-1}. Paroxetine was dissolved in the gel filtration buffer at a concentration of 15 mM and added to GRK2-$G\beta_1\gamma_2$C68S at final concentration of 1 mM. Paroxetine-GRK2-$G\beta_1\gamma_2$C68S was crystallized by the hanging drop method at 4 °C. Diffraction data was collected at the Advanced Photon Source at LS-CAT beam line 21-ID-F. Diffraction data was observed out to 2.07 Å spacings and was anisotropic (Supplementary

Table 2). The final model includes residues 30–484, 494–568, and 576–668 of GRK2, 2–340 of $G\beta_1$, and 8–64 of $G\gamma_2$. The atomic model and structure factors have been deposited with the Protein Data Bank as entry 3V5W.

Myocyte shortening measurements

Cardiac myocytes were isolated from LV free wall and septum of C57/Bl6 mice as described (49). All cells were used within 2–8 h of isolation. Myocytes were plated on laminin-coated coverslips and were bathed in HEPES-buffered (20 mM, pH 7.4) medium 199 containing 1.8 mM extracellular Ca^{2+}. When recording, coverslips containing myocytes were mounted in the Dvorak-Stotler chamber and bathed in 0.7 ml fresh medium. Cells were paced at 1 Hz and imaged with a variable field-rate camera (Zeiss IM35, Ionoptix) by both edge detection and sarcomere length. Peak contraction was measured as the percentage of cell shortening. Cells were treated with isoproterenol (Iso, 0.2 μM) for 2 min for the recording of contraction, with pretreatment of either PBS as vehicle or paroxetine (10 μM) for 10 min (49).

In vivo hemodynamic measurements

I*n vivo* cardiac hemodynamic function in C57/B6 mice was assessed 1 h after intra-peritoneal injection of either phospho-buffered saline (PBS, n=10) or paroxetine (10 mg kg^{-1}, n=14). In a separate study, mice received PBS (n=4) or fluoxetine (10 mg kg^{-1}, n=4) 1 h before catheterization. The physiological operator was blinded to the pre-treatment groups. Mice were anesthetized with a 2% Avertin and the right common carotid artery was isolated and cannulated with 1.4 French micro-manometer (Millar Instruments) as we have described previously (50). LV pressure, LV end-diastolic pressure (LVEDP) and heart rate (HR) were measured by this catheter advanced into the LV cavity, and data was recorded and analyzed on a PowerLab System (AD Instruments Pty Ltd.). These parameters as well as maximal values of the instantaneous first derivative of LV pressure ($+dP/dt_{max}$, as a measure of cardiac contractility) and minimum values of the instantaneous first derivative of LV pressure ($-dP/dt_{min}$, as a measure of cardiac relaxation) were recorded at baseline and after administration of the βAR agonist, isoproterenol (Iso, 0.1 to 10 ng) as described (50). Dose response curves from the various groups were statistically analyzed by a repeated measures ANOVA.

Supplementary Material

Refer to Web version on PubMed Central for supplementary material.

Acknowledgments

The authors thank M. Larsen, S. V. Roest, and P. Kirchoff and the Center for Chemical Genomics at the Life Sciences Institute, University of Michigan for their help in developing the aptamer-based high throughput screen and initial screening efforts. The authors also thank A. Waller, J. Jacob Strouse and M. B. Carter for their help with the Prestwick Chemical Library HTS and data analysis at the University of New Mexico Center for Molecular Discovery, which was supported by the Molecular Libraries Screening Network and the Molecular Libraries Probe program, and Dr. J. K. Northup for *Sepia* rhodopsin. This work was supported by the National Institute of Health (NIH) grants HL071818, HL086865 and DA030557 (to J.J.G.T.), DK19974 (to P.M.H.), and U54 MH084690 (to L.A.S). Data in myocytes and *in vivo* in mice was supported in part by NIH grants P01 HL075443 (Project 2), R37 HL061690 and R01 HL088503 (to W.J.K.). Use of the Cell and Molecular Biology Core of the Michigan Diabetes Research and Training Center was supported by DK20572. Use of the Advanced Photon Source was supported by the U. S. Department of Energy, Office of Science, Office of Basic Energy Sciences, under Contract No. DE-AC02-06CH11357. Use of the LS-CAT Sector 21 was supported by the Michigan Economic Development Corporation and the Michigan Technology Tri-Corridor (Grant 085P1000817).

$watermark-text
$watermark-text
$watermark-text

$watermark-text

$watermark-text

$watermark-text

References

1. Lefkowitz RJ, Stadel JM, Caron MG. Adenylate cyclase-coupled β-adrenergic receptors: structure and mechanisms of activation and desensitization. Annu Rev Biochem. 1983; 52:159–186. [PubMed: 6137187]
2. Gurevich EV, Tesmer JJ, Mushegian A, Gurevich VV. G protein-coupled receptor kinases: more than just kinases and not only for GPCRs. Pharmacol Ther. 2012; 133:40–69. [PubMed: 21903131]
3. Galetta F, Franzoni F, Bernini G, Poupak F, Carpi A, Cini G, Tocchini L, Antonelli A, Santoro G. Cardiovascular complications in patients with pheochromocytoma: a mini-review. Biomed Pharmacother. 2010; 64:505–509. [PubMed: 20580187]
4. Engelhardt S, Hein L, Wiesmann F, Lohse MJ. Progressive hypertrophy and heart failure in β_1-adrenergic receptor transgenic mice. Proc Natl Acad Sci U S A. 1999; 96:7059–7064. [PubMed: 10359838]
5. Liggett SB, Tepe NM, Lorenz JN, Canning AM, Jantz TD, Mitarai S, Yatani A, Dorn GW. Early and delayed consequences of β_2-adrenergic receptor overexpression in mouse hearts: critical role for expression level. Circulation. 2000; 101:1707–1714. [PubMed: 10758054]
6. Bristow MR, Ginsburg R, Minobe W, Cubicciotti RS, Sageman WS, Lurie K, Billingham ME, Harrison DC, Stinson EB. Decreased catecholamine sensitivity and β-adrenergic-receptor density in failing human hearts. N Engl J Med. 1982; 307:205–211. [PubMed: 6283349]
7. Eschenhagen T. β-adrenergic signaling in heart failure—adapt or die. Nat Med. 2008; 14:485–487. [PubMed: 18463653]
8. Ungerer M, Bohm M, Elce JS, Erdmann E, Lohse MJ. Altered expression of β-adrenergic receptor kinase and β_1-adrenergic receptors in the failing human heart. Circulation. 1993; 87:454–463. [PubMed: 8381058]
9. Ungerer M, Parruti G, Bohm M, Puzicha M, DeBlasi A, Erdmann E, Lohse MJ. Expression of β-arrestins and β-adrenergic receptor kinases in the failing human heart. Circ Res. 1994; 74:206–213. [PubMed: 8293560]
10. Koch WJ, Rockman HA, Samama P, Hamilton RA, Bond RA, Milano CA, Lefkowitz RJ. Cardiac function in mice overexpressing the β-adrenergic receptor kinase or a β-ARK inhibitor. Science. 1995; 268:1350–1353. [PubMed: 7761854]
11. Hata JA, Williams ML, Koch WJ. Genetic manipulation of myocardial β-adrenergic receptor activation and desensitization. J Mol Cell Cardiol. 2004; 37:11–21. [PubMed: 15242731]
12. Raake PW, Vinge LE, Gao E, Boucher M, Rengo G, Chen X, DeGeorge BRJ, Matkovich S, Houser SR, Most P, Eckhart AD, Dorn GWn, Koch WJ. G protein-coupled receptor kinase 2 ablation in cardiac myocytes before or after myocardial infarction prevents heart failure. Circ Res. 2008; 103:413–422. [PubMed: 18635825]
13. White DC, Hata JA, Shah AS, Glower DD, Lefkowitz RJ, Koch WJ. Preservation of myocardial β-adrenergic receptor signaling delays the development of heart failure after myocardial infarction. Proc Natl Acad Sci U S A. 2000; 97:5428–5433. [PubMed: 10779554]
14. Rockman HA, Chien KR, Choi DJ, Iaccarino G, Hunter JJ, Ross JJ, Lefkowitz RJ, Koch WJ. Expression of a β-adrenergic receptor kinase 1 inhibitor prevents the development of myocardial failure in gene-targeted mice. Proc Natl Acad Sci U S A. 1998; 95:7000–7005. [PubMed: 9618528]
15. Shah AS, White DC, Emani S, Kypson AP, Lilly RE, Wilson K, Glower DD, Lefkowitz RJ, Koch WJ. In vivo ventricular gene delivery of a β-adrenergic receptor kinase inhibitor to the failing heart reverses cardiac dysfunction. Circulation. 2001; 103:1311–1316. [PubMed: 11238278]
16. Rengo G, Lymperopoulos A, Zincarelli C, Donniacuo M, Soltys S, Rabinowitz JE, Koch WJ. Myocardial adeno-associated virus serotype 6-βARKct gene therapy improves cardiac function and normalizes the neurohormonal axis in chronic heart failure. Circulation. 2009; 119:89–98. [PubMed: 19103992]
17. Setyawan J, Koide K, Diller TC, Bunnage ME, Taylor SS, Nicolaou KC, Brunton LL. Inhibition of protein kinases by balanol: specificity within the serine/threonine protein kinase subfamily. Mol Pharmacol. 1999; 56:370–376. [PubMed: 10419556]

$watermark-text
$watermark-text
$watermark-text

18. Tesmer JJG, Tesmer VM, Lodowski DT, Steinhagen H, Huber J. Structure of human G protein-coupled receptor kinase 2 in complex with the kinase inhibitor balanol. J Med Chem. 2010; 53:1867–1870. [PubMed: 20128603]
19. Iino M, Furugori T, Mori T, Moriyama S, Fukuzawa A, Shibano T. Rational design and evaluation of new lead compound structures for selective βARK1 inhibitors. J Med Chem. 2002; 45:2150–2159. [PubMed: 12014953]
20. Winstel R, Ihlenfeldt HG, Jung G, Krasel C, Lohse MJ. Peptide inhibitors of G protein-coupled receptor kinases. Biochem Pharmacol. 2005; 70:1001–1008. [PubMed: 16102734]
21. Benovic JL, Stone WC, Caron MG, Lefkowitz RJ. Inhibition of the β-adrenergic receptor kinase by polyanions. J Biol Chem. 1989; 264:6707–6710. [PubMed: 2468660]
22. Ikeda, S.; Kaneko, M.; Ikeda, S.; Fujiwara, S.; Kaneko, M.; IKEDA, S.; LIMITED, TPC.; FUJIWARA, S. Takeda Pharmaceutical Company Limited. Cardiotonic Agent Comprising Grk Inhibitor, p A61K 45/00 A I; A61K 31/4196 A I; A4161K 4131/4433 A I; A4161K 4131/4409 A I; A4161K 4131/4439 A I; A4161K 4131/4506 A I; A4161K 4131/5377 A I; A4161P 4199/4104 A I; C4107D 4401/4104 A I. World Intellectual Property Organization; 2007.
23. Thal DM, Yeow RY, Schoenau C, Huber J, Tesmer JJG. Molecular mechanism of selectivity among G protein-coupled receptor kinase 2 inhibitors. Mol Pharmacol. 2011; 80:294–303. [PubMed: 21596927]
24. Mayer G, Wulffen B, Huber C, Brockmann J, Flicke B, Neumann L, Hafenbradl D, Klebl BM, Lohse MJ, Krasel C, Blind M. An RNA molecule that specifically inhibits G-protein-coupled receptor kinase 2 in vitro. RNA. 2008; 14:524–534. [PubMed: 18230760]
25. Hafner M, Vianini E, Albertoni B, Marchetti L, Grüne I, Gloeckner C, Famulok M. Displacement of protein-bound aptamers with small molecules screened by fluorescence polarization. Nat Protoc. 2008; 3:579–587. [PubMed: 18388939]
26. Tesmer VM, Lennarz S, Mayer G, Tesmer JJ. Molecular Mechanism for Inhibition of G Protein-Coupled Receptor Kinase 2 by a Selective RNA Aptamer. Structure. 2012
27. Shankaranarayanan A, Thal DM, Tesmer VM, Roman DL, Neubig RR, Kozasa T, Tesmer JJG. Assembly of high order $G\alpha_q$-effector complexes with RGS proteins. J Biol Chem. 2008; 283:34923–34934. [PubMed: 18936096]
28. Edwards BS, Zhu J, Chen J, Carter MB, Thal DM, Tesmer JJG, Graves SW, Sklar LA. Cluster cytometry for high-capacity bioanalysis. Cytometry Part A. 2012:419–429.
29. Benovic JL. Purification and characterization of β-adrenergic receptor kinase. Methods Enzymol. 1991; 200:351–362. [PubMed: 1659657]
30. Pitcher JA, Inglese J, Higgins JB, Arriza JL, Casey PJ, Kim C, Benovic JL, Kwatra MM, Caron MG, Lefkowitz RJ. Role of β γ subunits of G proteins in targeting the β-adrenergic receptor kinase to membrane-bound receptors. Science. 1992; 257:1264–1267. [PubMed: 1325672]
31. Carman CV, Som T, Kim CM, Benovic JL. Binding and phosphorylation of tubulin by G protein-coupled receptor kinases. J Biol Chem. 1998; 273:20308–20316. [PubMed: 9685381]
32. Pitcher JA, Hall RA, Daaka Y, Zhang J, Ferguson SS, Hester S, Miller S, Caron MG, Lefkowitz RJ, Barak LS. The G protein-coupled receptor kinase 2 is a microtubule-associated protein kinase that phosphorylates tubulin. J Biol Chem. 1998; 273:12316–12324. [PubMed: 9575184]
33. Mushegian A, Gurevich VV, Gurevich EV. The origin and evolution of G protein-coupled receptor kinases. PloS one. 2012; 7:e33806. [PubMed: 22442725]
34. Jones BW, Song GJ, Greuber EK, Hinkle PM. Phosphorylation of the endogenous thyrotropin-releasing hormone receptor in pituitary GH3 cells and pituitary tissue revealed by phosphosite-specific antibodies. J Biol Chem. 2007; 282:12893–12906. [PubMed: 17329249]
35. Johnson LN. Protein kinase inhibitors: contributions from structure to clinical compounds. Q Rev Biophys. 2009; 42:1–40. [PubMed: 19296866]
36. Kannan N, Haste N, Taylor SS, Neuwald AF. The hallmark of AGC kinase functional divergence is its C-terminal tail, a cis-acting regulatory module. Proc Natl Acad Sci U S A. 2007; 104:1272–1277. [PubMed: 17227859]
37. Boguth CA, Singh P, Huang C-c, Tesmer JJG. Molecular basis for activation of G protein-coupled receptor kinases. EMBO J. 2010; 29:3249–3259. [PubMed: 20729810]

$watermark-text

$watermark-text

$watermark-text

38. Williams ML, Hata JA, Schroder J, Rampersaud E, Petrofski J, Jakoi A, Milano CA, Koch WJ. Targeted β-adrenergic receptor kinase (βARK1) inhibition by gene transfer in failing human hearts. Circulation. 2004; 109:1590–1593. [PubMed: 15051637]
39. Casey LM, Pistner AR, Belmonte SL, Migdalovich D, Stolpnik O, Nwakanma FE, Vorobiof G, Dunaevsky O, Matavel A, Lopes CMB, Smrcka AV, Blaxall BC. Small molecule disruption of Gβγ signaling inhibits the progression of heart failure/novelty and significance. Circ Res. 2010; 107:532–539. [PubMed: 20576935]
40. Cohen P. Protein kinases--the major drug targets of the twenty-first century? Nat Rev Drug Discov. 2002; 1:309–315. [PubMed: 12120282]
41. Kluter S, Grutter C, Naqvi T, Rabiller M, Simard JR, Pawar V, Getlik M, Rauh D. Displacement assay for the detection of stabilizers of inactive kinase conformations. J Med Chem. 2010; 53:357–367. [PubMed: 19928858]
42. Chen CY, Dion SB, Kim CM, Benovic JL. β-adrenergic receptor kinase. Agonist-dependent receptor binding promotes kinase activation. J Biol Chem. 1993; 268:7825–7831. [PubMed: 8096517]
43. Bourin M, Chue P. Paroxetine: a review. CNS drug reviews. 2001
44. Mangin D, Healy D, Mintzes B. Paroxetine is associated with malformation during pregnancy. BMJ. 2011; 343
45. Jaber M, Koch WJ, Rockman H, Smith B, Bond RA, Sulik KK, Ross J Jr, Lefkowitz RJ, Caron MG, Giros B. Essential role of β-adrenergic receptor kinase 1 in cardiac development and function. Proc Natl Acad Sci U S A. 1996; 93:12974–12979. [PubMed: 8917529]
46. Roose SP, Laghrissi-Thode F, Kennedy JS, Nelson JC, Bigger JT Jr, Pollock BG, Gaffney A, Narayan M, Finkel MS, McCafferty J, Gergel I. Comparison of paroxetine and nortriptyline in depressed patients with ischemic heart disease. JAMA. 1998; 279:287–291. [PubMed: 9450712]
47. Gottlieb SS, Kop WJ, Thomas SA, Katzen S, Vesely MR, Greenberg N, Marshall J, Cines M, Minshall S. A double-blind placebo-controlled pilot study of controlled-release paroxetine on depression and quality of life in chronic heart failure. Am Heart J. 2007; 153:868–873. [PubMed: 17452166]
48. Lodowski DT, Barnhill JF, Pyskadlo RM, Ghirlando R, Sterne-Marr R, Tesmer JJG. The role of Gβγ and domain interfaces in the activation of G protein-coupled receptor kinase 2. Biochemistry. 2005; 44:6958–6970. [PubMed: 15865441]
49. Song J, Zhang X-Q, Wang J, Cheskis E, Chan TO, Feldman AM, Tucker AL, Cheung JY. Regulation of cardiac myocyte contractility by phospholemman: Na+/Ca2+ exchange versus Na+-K+-ATPase. American Journal of Physiology - Heart and Circulatory Physiology. 2008; 295:H1615–H1625. [PubMed: 18708446]
50. Gao E, Lei YH, Shang X, Huang ZM, Zuo L, Boucher M, Fan Q, Chuprun JK, Ma XL, Koch WJ. A novel and efficient model of coronary artery ligation and myocardial infarction in the mouse/ novelty and significance. Circ Res. 2010; 107:1445–1453. [PubMed: 20966393]

$watermark-text
$watermark-text
$watermark-text

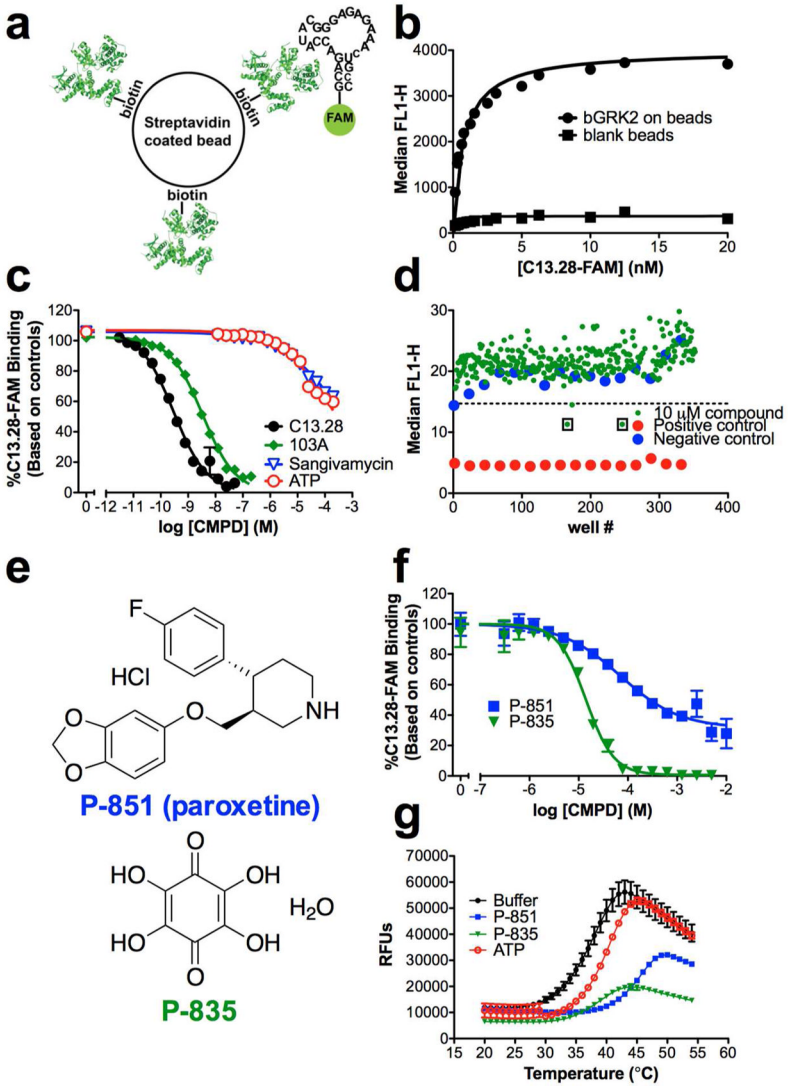

Figure 1. Identification of paroxetine as an inhibitor of GRK2

(**a**) Schematic of the GRK2-aptamer interaction used in the flow cytometry bead binding assay. Biotinylated GRK2 (bGRK2) was immobilized to streptavidin coated beads and bound by a fluorescein labeled aptamer (C13.28-FAM). (**b**) Representative binding and control isotherms for C13.28-FAM and bGRK2, wherein C13.28-FAM exhibited a dissociation constant (K_d) of 1.5 ± 0.9 nM (n=11) for bGRK2. (**c**) Competitive inhibition of C13.28-FAM binding by a panel of known GRK2 inhibitors. Data shown are representative mean values ± SEM of three or more experiments, performed in duplicate (see Table 1). (**d**) Primary screen identifying two small molecule inhibitors of the GRK2-aptamer interaction. Typical screening Z′ factors were ≥ 0.90 (0.62 for data shown) with 10 μM C13.28 as the positive control and DMSO as the negative control. Hits (boxed data points) were defined by their ability to decrease the fluorescence intensity below 3 σ from the negative (*i.e.* uninhibited) controls. (**e**) Structures of primary screening hits from the Prestwick Chemical Library. (**f**) Confirmation dose-response titrations of P-851 and P-835 against 2.0 nM C13.28-FAM as measured by the flow cytometry bead binding assay. (**g**) Changes in melting temperature (T_m) induced by incubation of 200 μM inhibitor or Mg^{2+}·ATP with

GRK2. Data shown are representative of three or more experiments performed in duplicate (**f**) or triplicate (**g**).

$watermark-text

$watermark-text

$watermark-text

$watermark-text
$watermark-text
$watermark-text

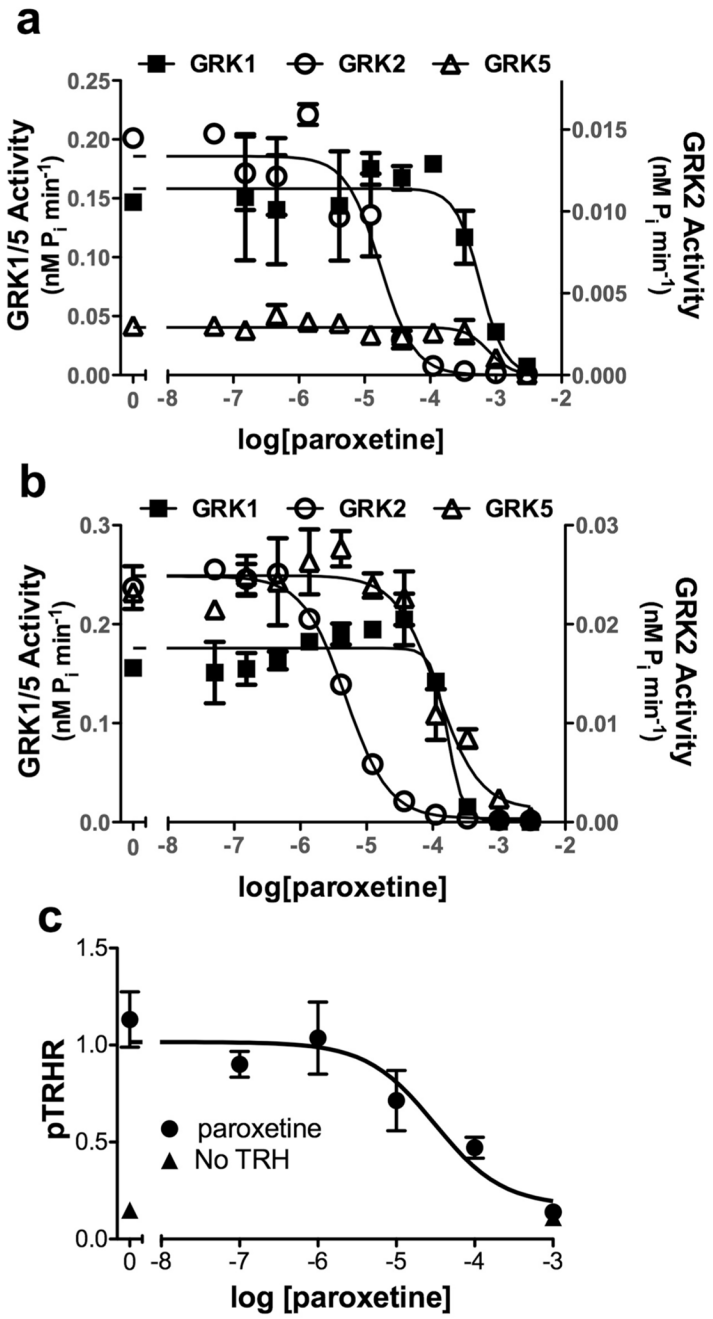

Figure 2. Paroxetine inhibits GRK2 activity *in vitro* and in living cells

Inhibition of GRK1, GRK2 and GRK5 mediated phosphorylation of (**a**) 500 nM bovine rod outer segments (ROS) or (**b**) 500 nM tubulin in the presence of 5 μM ATP. (**c**) Inhibition of GRK2-dependent phosphorylation of the thyrotropin-releasing hormone receptor (TRHR) by paroxetine. HEK293 cells were incubated for 45 min with indicated concentration of inhibitor and then stimulated with TRH for 15 s and agonist-dependent phosphorylation was evaluated using a phospho-site-specific antibody (34). Data points are the representative (**a** and **b**) or pooled (**c**) mean ± SEM values from three or more experiments performed in duplicate or triplicate.

$watermark-text

$watermark-text

$watermark-text

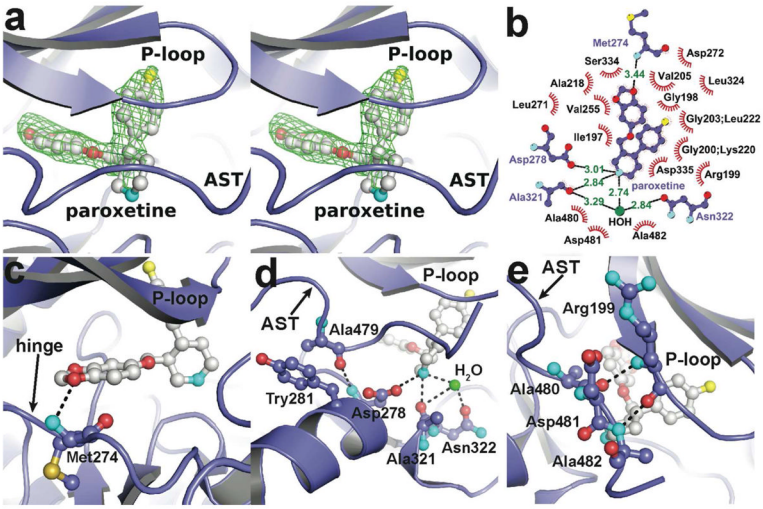

Figure 3. Atomic structure of the GRK2·paroxetine-Gβγ complex

(**a**) Stereo-view of paroxetine bound in the active site of GRK2. Electron density from an m|F_O| − D|F_C| omit map contoured at 3 σ is shown as a green cage. (**b**) Schematic of GRK2 interactions with paroxetine. Residues that form hydrogen-bonds (dashed lines) with paroxetine are shown in ball-and-stick representation with the interatomic distances shown in Å. Residues forming van der Waal interactions with paroxetine are shown as labeled arcs with radial spokes that point toward the ligand atoms they interact with. (**c** and **d**) Interactions of paroxetine with residues forming the adenine and ribose subsites, respectively. (**e**) Paroxetine binding stabilizes the AST region of GRK2, which contacts the inhibitor and forms novel interactions with the phosphate-binding loop (P-loop). Carbons for GRK2 and paroxetine are shown in slate and white, respectively. Nitrogens are colored cyan, oxygens red, and sulfur and fluorine yellow.

$watermark-text

$watermark-text

$watermark-text

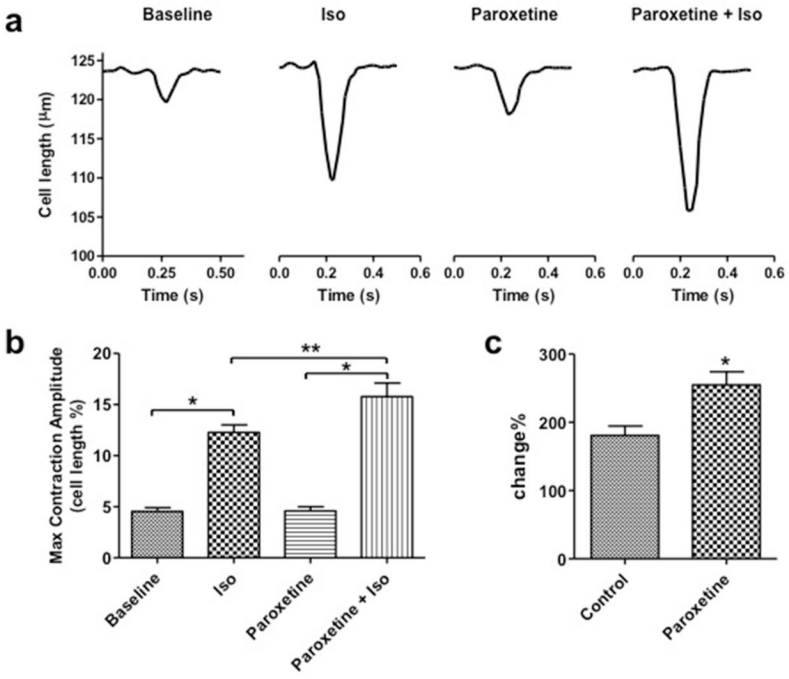

Figure 4. Paroxetine enhances βAR-mediated cardiomyocyte contractility *in vitro*

(**a**) Representative contraction tracings of single adult ventricular cardiomyocytes showing shortening with a basal twitch and after isoproterenol (Iso) stimulation, and then representative cell shortening basally and after Iso with paroxetine pre-treatment. (**b**) Quantitation of maximal single myocyte contraction amplitude under corresponding conditions. *, P<0.05 vs. Baseline; **, P<0.05 vs. Iso alone; n=18 myocytes in each condition. (**c**) Paroxetine treatment significantly increased the percent Iso-mediated change in myocyte contractility. *, P<0.05 paroxetine (plus Iso) vs. control (Iso alone).

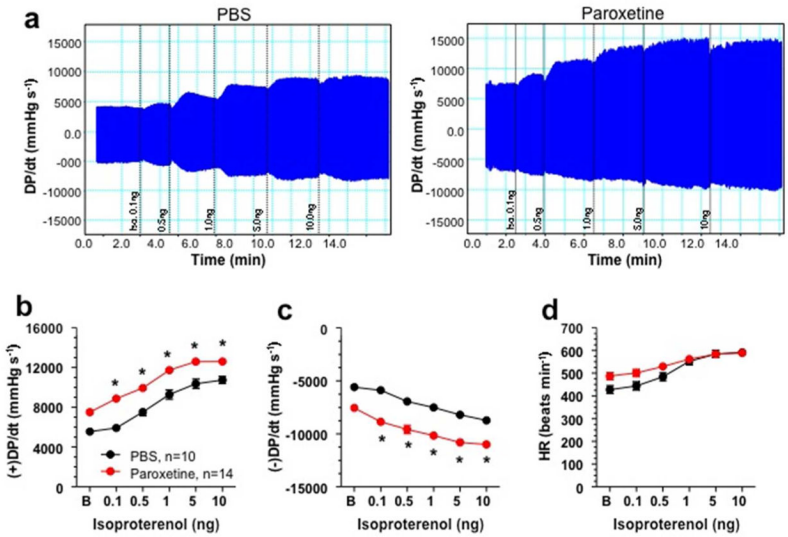

Figure 5. Paroxetine increases βAR-mediated *in vivo* cardiac contractility but does not affect heart rate

In vivo cardiac hemodynamic function was determined using Millar catheterization at 1 h after the treatment of phospho-buffered saline (PBS) or paroxetine (10 mg kg^{-1}). (**a**) Representative original left ventricular (LV) DP/dt data acquired from PBS or paroxetine pre-treated groups in response to increasing doses of isoproterenol (0.1–1.0 ng per mouse) (dotted lines). (**b**) The mean ± SEM of baseline (B) and isoproterenol dose response (in ng per mouse) of maximal LV +dP/dt (+DP/dt). *, P<0.05 paroxetine vs. PBS (ANOVA), n=14 and 10 mice per group, respectively. (**c**) Mean ± SEM of baseline (B) and isoproterenol dose response of minimal LV −dP/dt (+DP/dt) as a measure of cardiac relaxation. *, P<0.05 Paroxetine vs. PBS (ANOVA), n=6–9 mice per group. (**d**) Heart rate (HR) values (mean ± SEM) of mice at baseline (B) and after isoproterenol.

$watermark-text
$watermark-text
$watermark-text

$watermark-text $watermark-text $watermark-text

Table 1

Summary of ligand competition and Thermofluor data

	competition (2 nM C13.28-FAM)			ΔT_m (°C)		
	pIC_{50}	**n_H**	***n***	**GRK1**	**GRK2**	**GRK5**
C13.28	9.3 ± 0.5	−0.9	4	N.D.	N.D.	N.D.
103A	8.6 ± 0.4	−0.8	6	6.2 ± 0.6[a]	15.5 ± 0.7[a]	3.6 ± 0.4[a]
ATP	4.3 ± 0.3	−0.7	4	18.0 ± 1.5	4.9 ± 1.6	7.2 ± 1.1
sangivamycin	5.0 ± 0.3	−1.0	3	N.D.	N.D.	N.D.
P-835	5.5 ± 0.4	−1.6	4	−0.14 ± 0.1	1.2 ± 0.8	−0.007 ± 0.3
paroxetine	4.5 ± 0.2	−0.7	4	1.5 ± 1.1	7.8 ± 1.1	−0.4 ± 0.3

Values represent the mean ± SEM of *n* experiments, performed in duplicate (flow cytometry bead binding) or triplicate (Thermofluor). ΔT_m, change in melting temperature; n_H, Hill slope; N.D., not determined. With the exception of 103A, ligands in the Thermofluor assay were added to a final concentration of 200 μM.

[a]Previously determined (23).

$watermark-text $watermark-text $watermark-text

Table 2

Selectivity of paroxetine for representative GRK Subfamily members

	GRK1			GRK2			GRK5		
	pIC_{50}	**n_H**	***n***	**pIC_{50}**	**n_H**	***n***	**pIC_{50}**	**n_H**	***n***
ROS	3.5 ± 0.07	−2.0	*3*	4.7 ± 0.04	−1.0	*4*	3.6 ± 0.3	−3.6	*3*
Tubulin	3.8 ± 0.05	−3.4	*2*	5.6 ± 0.07	−1.1	*2*	3.9 ± 0.06	−1.3	*2*

Values represent the average pIC_{50} ± SEM of *n* experiments and Hill slopes (n_H) for inhibition of GRK mediated phosphorylation by paroxetine, performed in duplicate using 5 μM ATP and 500 nM bovine rhodopsin (ROS) or tubulin as substrates.

ACS Chem Biol. Author manuscript; available in PMC 2013 November 16.

$watermark-text

$watermark-text

$watermark-text

Table 3

Paroxetine enhances βAR-mediated cardiomyocyte contractility

	Control	Paroxetine	P-value
Baseline before isoproterenol			
Max. contraction amplitude (% cell length)	4.6 ± 0.4	4.5 ± 0.4	0.988
Max. shortening velocity (μm s^{-1})	−0.81 ± 0.07	−0.77 ± 0.09	0.725
Max. relengthening velocity (μm s^{-1})	0.60 ±0.07	0.58 ± 0.08	0.834
Half-time of relaxation (ms)	54.1 ± 3.1	65.9 ± 7.3	0.143
After isoproterenol			
Max. contraction amplitude (% cell length)	12.3 ± 0.7	15.8 ± 1.3	0.0191
% increase in contraction amplitude	180.9 ± 13.8	260.2 ± 19.0	0.0018

Values represent the mean ± SEM for n=18 cardiomyocytes.